Energy 219 (2021) 119566

Contents lists available at ScienceDirect

Energy

journal homepage: www.elsevier.com/locate/energy

Thermal-hydraulic performance analysis of a novel parabolic trough receiver with double tube for solar cascade heat collection

Peng Liu, Zhimin Dong, Hui Xiao, Zhichun Liu, Wei Liu*

School of Energy and Power Engineering, Huazhong University of Science and Technology, Wuhan, 430074, China

ARTICLE INFO

Article history:
Received 3 August 2020
Received in revised form
20 October 2020
Accepted 7 December 2020
Available online 11 December 2020

Keywords:
Solar cascade heat collection
Parabolic trough receiver
Double tube
Heat collecting performance

ABSTRACT

The utilization of solar energy is of great significance to alleviate energy shortage and environmental problems. In view of the different thermal grade requirements of electricity production and water desalination in remote arid areas as well as to improve the performance of the parabolic trough receiver (PTR), a novel solar cascade heat collection system based on a PTR with double tube and two heat transfer fluids (HTF) is proposed in this paper. A three-dimensional model is developed to simulate and investigate the temperature distribution, heat transfer and flow characteristics and heat collecting performance of the novel system. Moreover, the effects of the operating parameters on the performance are studied in details. The temperatures of the absorber tube are significantly reduced over the plain PTR, and the heat transfer coefficient on the absorber inner surface is enhanced about 50% with 2.5–6.8 times increment in total pumping work. In addition, the heat loss reduced up to 43.1%, thus, the maximum improvement of the total thermal efficiency reaches up to 1.5%. Within the parameters considered in this study, the proportions of the high and low temperature heat gains are ranged in 39.01–62.92% and 28.37–8.86% of the incident solar energy, respectively.

1. Introduction

With the prosperity of the world economy and the rapid consumption of fossil fuel, the contradiction between the growing energy demand and multiple problems, such as fossil fuel depletion, global warming, environment pollution, etc. is becoming increasingly serious [1–3]. Solar energy, a clean and renewable energy, is the world's most abundant energy and has huge potential to meet the growing energy demand and alleviate the above contradiction [4]. Solar energy utilization is divided into photothermal conversion and photoelectric conversion [5]. Solar thermal utilization such as concentrating solar thermal power generation technology is a safe, reliable, clean and renewable energy technology with broad application prospects, which has become an international consensus to accelerate its large-scale development [6]. Concentrating solar thermal collector is the core component of solar thermal utilization technology. And there are four main types of concentrating solar thermal collectors including parabolic trough collector (PTC), linear Fresnel reflector, heliostat field collector and parabolic dish collector [7]. Among them, the PTC is the most mature solar concentrating technology with the advantages of easy modularization, wide applications, and easy matching with other renewable energy sources. Thus, it has drawn extensive attention and research interest all over the world [8].

Parabolic trough receiver (PTR), the key component of PTC, can absorb the concentrated solar irradiation and convert it into heat of heat transfer fluid (HTF) with temperature up to 400 °C, which can be used for electricity production [9]. Recently, for the purposes of reducing the investment cost and improving the overall utilization efficiency of solar energy, the PTC is developing towards higher concentration ratio and operating temperature [10,11]. However, the highly non-uniform heat flux loaded on the absorber tube outer surface will induce excessively high local temperature and large circumferential temperature gradient in the absorber tube at the same time. Consequently, the PTR may suffer several problems, including the local high-temperature burnout, significant increase in heat loss [12], degeneration of HTF and selective coating caused by excessive high temperature, and structural instability and destruction induced by the extremely increase in thermal stress [13,14]. All of these problems bring challenges to the long-term efficient and safe operation of the PTC. Heat transfer enhancement technology, which can increase the heat transfer rates

* Corresponding author.
E-mail address: w_liu@hust.edu.cn (W. Liu).

https://doi.org/10.1016/j.energy.2020.119566
0360-5442/

between the absorber tube and HTF and reduce the thermal losses and stress, has the advantages of low cost, excellent performance and simple structure. Therefore, it is one of the most potentially effective method to overcome these problems [15]. Nanofluids and turbulators are two main categories of heat transfer enhancement technologies for PTR [16]. Nanofluids is the technology that focuses on improving properties of the fluids and heat transfer performance by adding and dispersing metallic nanoparticles such as Al_2O_3 [17], CuO [18], and Cu [19] into based fluids such as thermal oil and molten salt [20], and has been widely researched [21,22]. However, several drawbacks of nanofluids, including high production cost, agglomeration and instability, are still need to be overcome with long-term effort for its large-scale industrial applications [23]. In contrast, because of its low cost and easy manufacture and installation, turbulators such as twisted tape inserts [24], perforated plate inserts [25], wavy-tape insert [26], conical strip inserts [27], helical screw-tape inserts [28], etc., and modifications of absorber tube inner surface such as internal longitudinal fins [29], unilateral longitudinal vortex generators [30], corrugated tube [31,32], ribbed absorber tube [33], helically finned tube [34], which focus on disturbing the fluid and promoting the flow mixing so as to enhance the heat transfer, have drawn increasing research interest. For example, Chang et al. [35] reported a numerical study of a PTR with eccentric rod inserts. They found that the enhanced PTR obtains 10–642% increment in heat transfer coefficient and 1.68–1.84 times performance evaluation criteria over a plain PTR. Song et al. [28] studied the performance of a PTR fitted with the helical screw-tape insert, and they found that the heat loss, peak temperature and temperature gradient of the PTR can be significantly reduced. Bellos et al. [36] examined performance of different internally finned absorber tubes in PTR and obtained 0.82% and 65.8% increments in thermal efficiency and heat transfer coefficient, respectively. Wang et al. [31] evaluated the heat transfer and thermal performance of PTR with corrugated tube. They achieved up to 8.4% increment in heat transfer coefficient and up to 13.1% reduction in thermal strain.

In addition to being used for electricity production, solar heat can also be used in many other applications, such as desalination, domestic heat, etc. [37]. Among them, the desalination technologies driven by solar energy have been extensively researched all over the world [38–41]. In some remote arid regions like North Africa or islands, there are great demands for both electricity and fresh water. Solar energy has huge potential to meet these two demands. In recent, the combined power production and water desalination by using concentrated solar energy has drawn increasing attention [42]. In view of different grades of thermal energy being required for electricity generation and water desalination, a novel parabolic trough receiver with double tube for solar cascade heat collection is proposed in this study. As shown in Fig. 1, the novel solar cascade heat collecting system is composed of a traditional PTR and an eccentric inner tube. So it can be transformed from the traditional PTR and easily put into practice at low cost. In addition, the inner tube can work as a rod insert in Ref. [35], which can enhance the heat transfer coefficient and improve the thermal-mechanical performance of PTR. In this system, seawater or brine is selected as the low temperature HTF, which flows in the inner tube and provides low-grade thermal energy for desalination and/or salinity gradient energy harvesting [43]; while Syltherm-800 oil is selected as high temperature HTF between the absorber tube inner surface and outer surface of the inner tube, which provides high-grade thermal energy for electricity generation. A numerical model is established to study and analyze the thermal-

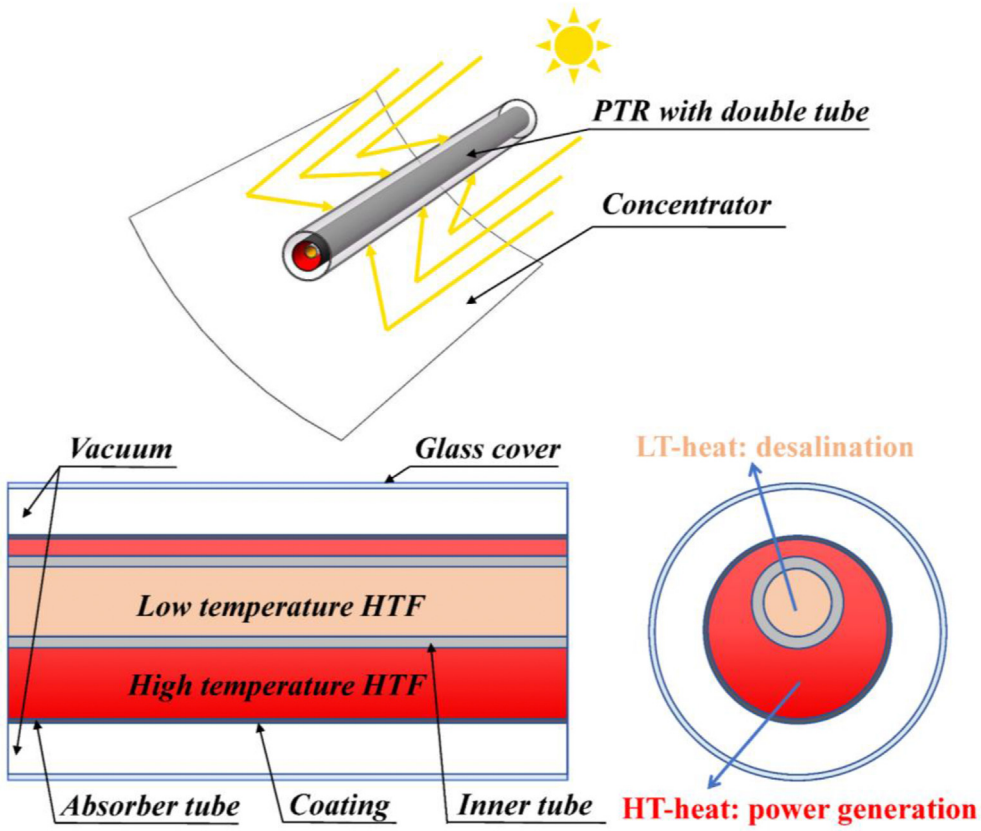

Fig. 1. Sketch map of a PTR with double tube for solar cascade heat collection.

hydraulic performance of the solar cascade heat collecting system. Flow structure and temperature distribution, heat transfer and flow characteristics, as well as heat collecting performance under different parameters are also investigated in details. This study may provide technical guidance for the cascade comprehensive development and utilization of solar thermal energy.

2. Model description

2.1. Physical model

Fig. 2 (a) and (b) display the front view and left view of the PTR with double tube respectively. A standard LS2 PTC [28] with full length of 7.8 m is applied in this work, which consists of a absorber tube with inner (d_{ri}) and outer (d_{ro}) diameters of 66 and 70 mm, a glass cover tube with inner (d_{gi}) and outer (d_{go}) diameters of 109 and 115 mm, and an annular vacuum zone in the middle. An inner tube with the same length of the LS2 PTC is fitted in the absorber tube with an eccentric distance (e) of 10 mm in y direction. And its inner (d_{ii}) and outer (d_{io}) diameters are set to 20 and 30 mm, respectively. Considering the symmetry of the PTR with double tube in y-direction, only half of the PTR is taken as the calculation domain, as shown in Fig. 2 (b).

The thermal network of the PTR with double tube is presented in Fig. 1 (c). All of the three types of heat transfer modes: heat conduction, heat convection and heat radiation, are simultaneously considered in this model. The concentrated solar irradiation is absorbed by the selective coating on the absorber tube outer surface and turned into heat flux. In the present work, a circumferential non-uniform heat flux under direct normal irradiance (DNI) of 1000 W/m^2 from He's research [44], as shown in Fig. 1 (d), is loaded on the absorber tube outer surface to represent the solar energy input (Q_{soalr}). Most of the heat is transferred to the absorber tube inner surface through conduction and then taken away by the HT-HTF through convection. Then part of this heat is transferred to the LT-HTF by conduction of inner tube and convection between the LT-HTF and the inner tube. Another small amount of heat is transferred to the glass cover inner surface through radiation and conduction. Finally, this part of the heat is lost to the ambient and the sky by heat convection and radiation, respectively. Syltherm-800 oil [26] and water are applied as the HT-HTF and LT-HTF, whose temperature-dependent properties are listed in Table 1, respectively. Wherein, the temperature-dependent properties of the water are fitted into polynomials based on the data from the reference [45]. The materials of absorber tube and glass cover are selected as the stainless steel (321H) with the thermal conductivity of 25 W/(m·K) [28] and Pyrex with the thermal conductivity of 1.2 W/(m·K) [46], respectively. In addition, the inner tube is made up of porous zirconia ceramic with the effective thermal conductivity of 0.4 W/(m·K) [47], which has good high temperature resistance and low thermal conductivity to maintain a large temperature difference between the inner and outer surfaces of the inner tube. The properties of these solid materials applied in this study are also listed in Table 1.

No slip condition is employed to the interface of convective heat transfer including both sides of the inner tube and the absorber tube, and outer surfaces of the glass cover. The emissivity on surfaces of the glass cover is set to 0.89 [26,28]. On the outer surface of the glass cover, a mixed boundary condition of convection and radiation is adopted. Among them, the assumption of uniform convective heat transfer coefficient, which is defined as Eq. (1) [48], is applied, where the V_w is the wind speed and takes a value of 2.5 m/s. And the heat transfer through radiation is calculated by Stefan-Boltzmann law. In the present work, the temperatures of the ambient and the sky are set to 298 K and 290 K respectively, where the sky temperature is 8 K lower than that of the ambient [49]. In addition, selective coating is applied on the absorber tube outer surface. And its temperature-dependent emissivity is formulated as Eq. (2) [50], where T is the local temperature of the surface in K. Different inlet temperatures and mass flow rates of the HT-HTF and LT-THF are studied in the present work to determine their effects on the performance of the solar cascade heat collecting system. Five inlet temperatures ($T_{in,oil}$ = 400, 450, 500, 550, 600 K) and five mass flow rates (M_{oil} = 0.5, 0.6, 0.7, 0.8, 0.9 kg/s) for the HT-THF as well as five inlet temperatures ($T_{in,water}$ = 298.15, 308.15, 318.15, 328.15, 338.15 K) and mass flow rate (M_{water} = 0.06, 0.09, 0.12, 0.15, 0.18 kg/s) for the LT-HTF are selected to be investigated and analyzed in this study.

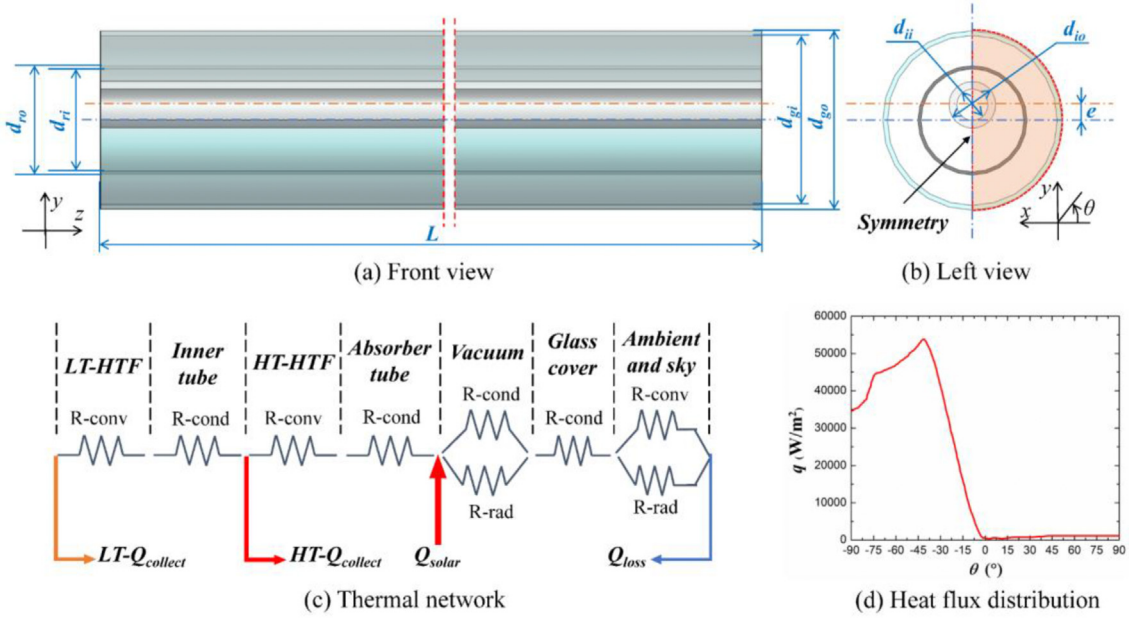

Fig. 2. Schematic of the PTR with double tube, thermal network and heat flux distribution.

Table 1
Properties of the materials applied in the present work.

Fluid Materials	HT-HTF (Syltherm-800) (Temperature-dependent properties)	LT-HTF (Water) (Temperature-dependent properties)
ρ (kg/m^3)	$-6.0616 \times 10^{-4}T^2$ - $4.1535 \times 10^{-1}T + 1.1057 \times 10^3$	$1.772 \times 10^{-5}T^3$ - $2.067 \times 10^{-2}T^2 + 7.355T + 1.71956 \times 10^2$
c_p (J/(kg·K))	$1.7080T + 1.1078 \times 10^3$	$1.471 \times 10^{-6}T^4 - 1.973 \times 10^{-3}T^3 + 1.005T^2$ - $2.2965 \times 10^2T + 2.3978 \times 10^4$
λ (W/(m·K))	$-5.7534 \times 10^{-10}T^2$-$1.8752 \times 10^{-4}T + 1.9002 \times 10^{-1}$	$3.419 \times 10^{-8}T^3$ - $4.581 \times 10^{-5}T^2 + 2.014 \times 10^{-2}T - 2.229$
μ (kg/(m·s))	$6.6720 \times 10^{-13}T^4$-$1.5660 \times 10^{-9}T^3 + 1.3882 \times 10^{-6}T^2$- $5.5412 \times 10^{-4}T + 8.4866 \times 10^{-2}$	$4.078 \times 10^{-11}T^4 - 5.502 \times 10^{-8}T^3 + 2.789 \times 10^{-5}T^2$- $6.302 \times 10^{-3}T + 0.536574$

Solid Materials	Glass cover (Pyrex)	Absorber tube (Stainless steel)	Inner tube (Porous zirconia ceramic)
ρ (kg/m^3)	2230	7650	5700
c_p (J/(kg·K))	900	460	500
λ (W/(m·K))	1.2	25	0.4

$$h_w = 4V_w^{0.58} d_{go}^{-0.42} \tag{1}$$

$$\xi = 0.000327T - 0.065971 \tag{2}$$

2.2. Computational methods

In this study, the fluid flow and heat transfer processes of the HT- and LT-HTFs are assumed to be steady-state and turbulent as the Reynolds numbers being larger than 5000. The realizable k-ε two-equation turbulence model, which is good at predicting the flow features [51], is adopted in this work, and the corresponding governing equations are expressed as below [52].

Continuity equation:

$$\frac{\partial(\rho u_i)}{\partial x_i} = 0 \tag{3}$$

Momentum equation:

$$\frac{\partial(\rho u_i u_j)}{\partial x_i} = -\frac{\partial P}{\partial x_i} + \frac{\partial}{\partial x_j}\left((\mu+\mu_t)\left(\frac{\partial u_i}{\partial x_j}+\frac{\partial u_j}{\partial x_i}\right) - \frac{2}{3}(\mu+\mu_t)\frac{\partial u_i}{\partial x_i}\delta_{ij} - \rho\overline{u_i' u_j'}\right) \tag{4}$$

Energy equation:

$$\frac{\partial(\rho u_i T)}{\partial x_i} = \frac{\partial}{\partial x_i}\left(\frac{\mu}{\mathrm{Pr}} + \frac{\mu_t}{\mathrm{Pr}_t}\right)\frac{\partial T}{\partial x_i} \tag{5}$$

Equation of Turbulent kinetic energy k

$$\frac{\partial(\rho u_i k)}{\partial x_i} = \frac{\partial}{\partial x_i}\left(\left(\mu + \frac{\mu_t}{\sigma_k}\right)\frac{\partial k}{\partial x_i}\right) + \Gamma - \rho\varepsilon \tag{6}$$

Equation of turbulent energy dissipation ε

$$\frac{\partial(\rho u_i \varepsilon)}{\partial x_i} = \frac{\partial}{\partial x_i}\left(\left(\mu + \frac{\mu_t}{\sigma_\varepsilon}\right)\frac{\partial \varepsilon}{\partial x_i}\right) + c_1\Gamma\varepsilon - \rho c_2 \frac{\varepsilon^2}{k + \sqrt{\nu\varepsilon}} \tag{7}$$

where ρ, u, P and T are the densities, velocity components, pressures and temperatures of the HTFs, respectively. μ and Pr represent the viscosities and the Prandtl numbers of the HTFs, respectively. μ_t represent the turbulent viscosities, and Pr_t, σ_k and σ_ε are the turbulent Prandtl numbers for T, k and ε. The generation of turbulence kinetic energy (Γ) in Eq. (7) is defined as:

$$\Gamma = -\overline{u_i u_j}\frac{\partial u_i}{\partial x_i} = \mu_t\left(\frac{\partial u_i}{\partial x_j} + \frac{\partial u_j}{\partial x_i}\right)\frac{\partial u_i}{\partial x_i} \tag{8}$$

Software ANSYS Fluent 16.0 with the double precision pressure based solver, which is based on the finite volume method (FVM), is employed for numerical calculation. The governing equations are discretized with second order upwind scheme. The SIMPLE algorithm is adopted to achieve the coupling between velocity and pressure. In addition, to capture the high resolution of gradients near the inner and outer surfaces of the inner tube and the inner surface of the absorber tube, the enhanced wall treatment method is applied. Discrete Ordinates (DO) radiation model is selected to simulate the radiation heat transfer through the annular space. The convergence criteria in this study are that the relative residuals are less than 10^{-5} for continuity equation and 10^{-7} for the other equations.

2.3. Parameter definitions

The Reynolds number (Re), average heat transfer coefficient (h), average Nusselt number (Nu) and friction factor (f) are defined as below [53]:

$$Re = \frac{\rho u d}{\mu} \tag{9}$$

$$h = q_w \Big/ \left(T_w - T_f\right) \tag{10}$$

$$Nu = hd/\lambda \tag{11}$$

$$f = \frac{2\Delta P_L d}{\rho u^2} \tag{12}$$

where T_f is the bulk temperature of the HTFs, and ρ, μ and λ are the densities, viscosities and thermal conductivities of the HTFs at T_f. $q_w$and T_w represent the average heat flux and temperature on the inner tube or absorber tube inner surface, respectively. d is the inner diameter of the absorber tube or inner tube, and ΔP_L is the pressure drop per unit distance in the flow direction. u is the average velocities of the HTFs defined as below:

$$u = \frac{4M}{\rho\pi d^2} \tag{13}$$

where M represent the mass flow rates of the HTFs.

The heat collecting efficiency [24] (η) is defined as Eq. (14) to evaluate the heat collecting performance of the PTR with double tube.

$$\eta = \frac{Q_c}{A_a \cdot DNI} \tag{14}$$

In which, A_a is the collector's aperture area, and Q_c is the

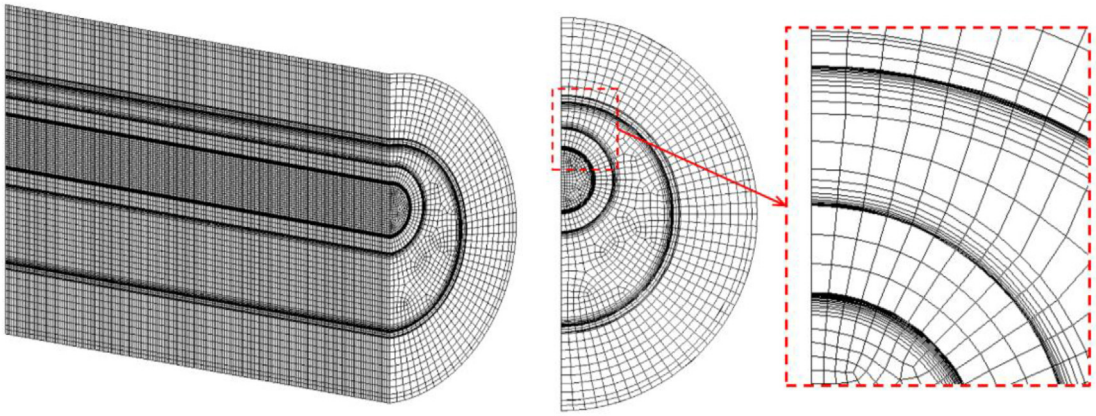

Fig. 3. Grid system.

Table 2
Grid independence test results.

Grid system	1	2	3
Grid number	1830400	4402320	7934550
Efficiency (%)	70.45	70.44	70.44
Heat loss (W/m)	130.65	133.40	133.33
T_{max} on absorber tube (K)	623.46	625.02	624.97
Nu of absorber tube	275.84	266.06	266.34
f of absorber tube	0.09379	0.09327	0.09328
Nu of inner tube	48.00	47.47	47.32
f of inner tube	0.03748	0.03706	0.03694

collected heat that including high temperature collecting heat (*HT-*$Q_{collect}$) and low temperature collecting heat (*LT-*$Q_{collect}$).

2.4. Grid system and independence test

Grid system that established by using software Gambit 2.4.6 is presented in Fig. 3. Highly refined meshes are adopted in the boundary region near the inner and outer surfaces of the inner tube and the inner surface of the absorber tube to ensure that y^+ less than 1 and guarantee computational accuracy. Three grid systems with grid numbers of 1830400, 4402320 and 7934550 are applied to conduct the grid independence test in this work. The results of heat collecting efficiency, heat loss, the maximum temperature of absorber tube as well as Nusselt numbers and friction factors for both absorber tube and inner tube at different grid numbers are listed in Table 2. It is observed that the grid system with 4402320 cells is sufficiently dense as its relative deviations with the finer mesh being limited in 0.3%. Therefore, the grid system 2 is applied to the following simulation in this work.

3. Model validation

To verify the accuracy of the computational model and method in the present work, the Gnielinski correlation for the Nusselt number and the Petukhov's correlation for friction factor [54], which are expressed as Eqs. (15) and (16), are adopted to verify the simulation on heat transfer and flow characteristics of the oil in the plain absorber tube and the water in the inner tube. The comparisons of *Nu* and *f* between the numerical results and the correlations for a plain PTR and the LT-HTF in the inner tube are displayed in Fig. 4 (a) and (b), respectively. It is clear that the heat transfer and flow characteristics agree well with the correlations, with the relative deviations of *Nu* and *f* for the oil in PTR with plain tube being located within ±3.4% and ±2.2%, and those for the water in

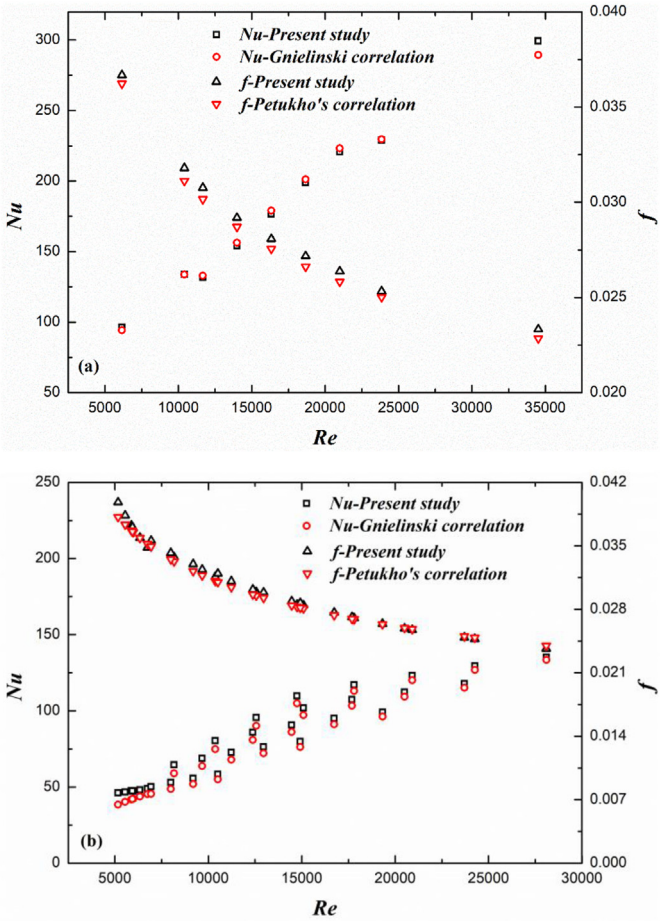

Fig. 4. Comparisons of *Nu* and *f* between this work and the correlations: (a) oil in the plain absorber tube; (b) water in the inner tube.

the inner tube within ±19.8% and ±4.3%, respectively. Moreover, comparisons of temperature gain and heat collecting efficiency of a PTR with plain absorber tube between the experimental data from Dudley et al. [55] and the numerical results are carried out. The comparison results are listed in Table 3. It is found that the numerical results show a good agreement with the experimental data, as the deviations are within ±3.58% and ±4.08% for temperature gain and heat collecting efficiency, respectively. Therefore, it is considered that the physical model and computational methods

Table 3
Validation with experimental data.

Case	1	2	3	4	5	6	7	8
DNI(W/m^2)	933.7	968.2	982.3	909.5	937.9	880.6	920.9	903.2
Wind speed(m/s)	2.6	3.7	2.5	3.3	1.0	2.9	2.6	4.2
Air temperature (°C)	21.2	22.4	24.3	26.2	28.8	27.5	29.5	31.1
Flow rate (L/min)	47.70	47.78	49.10	54.70	55.50	55.60	56.80	56.30
$T_{in,oil}$ (°C)	102.2	151.0	197.5	250.7	297.8	299.0	379.5	355.9
Temperature gain-Exp (°C)	21.80	22.02	21.26	18.70	19.10	18.20	18.10	18.50
Temperature gain-Present study (°C)	21.98	21.23	21.79	18.33	18.80	17.59	18.03	17.92
Error Temperature gain (%)	0.84	−3.58	2.52	−1.95	−1.52	−3.37	−0.40	−3.11
Efficiency-Exp (%)	72.51	70.90	70.17	70.25	67.98	68.92	62.34	63.83
Efficiency-Present study (%)	73.44	68.01	69.76	68.66	67.01	66.75	61.31	63.45
Error efficiency (%)	1.29	−4.08	−0.59	−2.27	−1.42	−3.15	−1.65	−0.59

applied in this paper are reliable and accurate.

$$Nu = \frac{(f/8)(\mathrm{Re}-1000)\mathrm{Pr}}{1+12.7(f/8)^{0.5}\left(\mathrm{Pr}^{2/3}-1\right)}\left[1+\left(\frac{d}{L}\right)^{2/3}\right] \tag{15}$$

$$f = (0.790\ln\mathrm{Re}-1.64)^{-2} \tag{16}$$

4. Results and discussion

4.1. Flow structure and temperature distribution

Fig. 5 (a) and (b) show the comparisons of velocity and temperature distributions on the cross-section (z = 3.9 m) at $T_{in,oil}$ = 400 K, M_{oil} = 0.7 kg/s, $T_{in,water}$ = 298.15 K and M_{water} = 0.06 kg/s, respectively. In PTR with double tube, due to the insertion of the inner tube, the flow cross-sectional area of HT-HTF (oil) is reduced and its velocity is significantly increased when compared to that of the plain PTR under the same mass flow rate of the oil. Therefore, the convective heat transfer performance between the oil and the absorber tube inner surface is effectively enhanced. Furthermore, the fluid velocity gradient near the inner surface of the lower half of the absorber tube is markedly increased, as shown in Fig. 5 (a). As a result, a higher local heat transfer coefficient in low half part of the absorber tube is obtained. Thus, the high heat flux from concentrated solar radiation in this region can be taken away more efficiently by the HTF. Consequently, the circumferential temperature gradient of the absorber tube is dramatically reduced compared to that of a plain PTR, as shown in Fig. 5 (b). Fig. 6 gives the temperature contours on the outer surfaces of the absorber tube in a plain PTR and PTR with double tube. It is obviously that the PTR suffers an excessively high peak temperature and large circumferential temperature gradient, which may induce several adverse impacts on the safe and efficient operation of the PTC, such as the degradation of the HTF and selective coating at high temperature, excessive thermal stress in the absorber tube and its deformation caused by the large temperature gradient, etc. In contrast, the PTR with double tube obtains apparently lower peak temperature and circumferential temperature gradient, which is beneficial for improving the thermal and mechanical performance of the PTR. In addition, the inner tube can increase the overall bending strength of the PTR and thus further reducing its thermal deformation so as to improve the mechanical performance.

Effects of the inlet temperatures and mass flow rates of the oil (HT-HTF) and water (LT-HTF) on the maximum temperature (T_{max}) and temperature difference (ΔT) of the absorber tube are displayed in Fig. 7 (a)-(c). With the inlet temperature of the oil increasing from 400 to 600 K, both the T_{max} of the absorber tubes in plain PTR and the PTR with double tube increase and the reduction in T_{max} between the PTR with double tube and the plain PTR decreases gradually from 66 to 36 K, as shown in Fig. 7 (a). In addition, as the viscosity of the oil decreases with the increasing temperature, its convective heat transfer performance improves under the same mass flow rate. Therefore, the ΔT of the PTRs decrease with the augment of the oil inlet temperature. From Fig. 7 (b), both the T_{max}

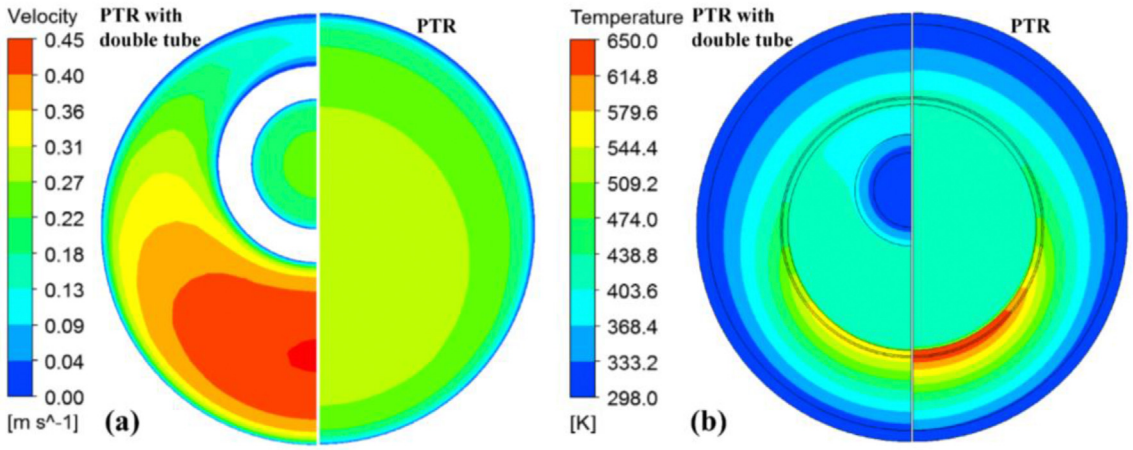

Fig. 5. Comparisons of the velocity and temperature distributions on the cross-section (z = 3.9 m) between a PTR and PTR with double tube: (a) velocity; (b) temperature.

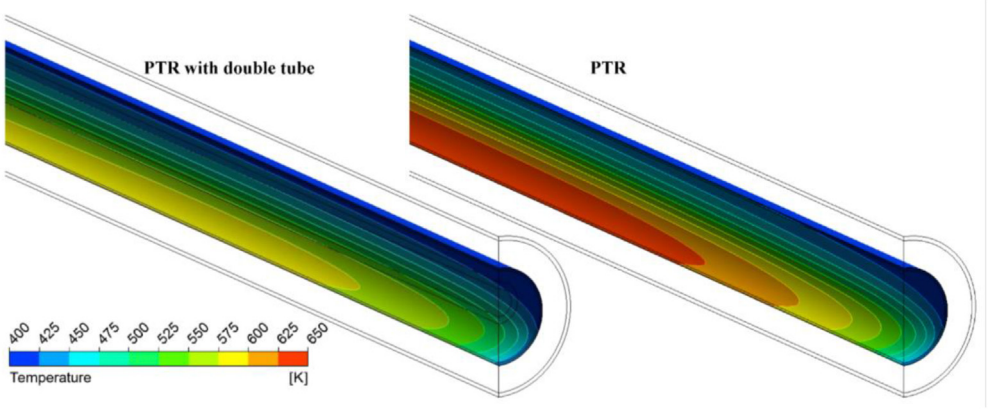

Fig. 6. Temperature contours on the outer surfaces of the absorber tube near the inlet at $T_{in,oil}$ = 400 K, M_{oil} = 0.7 kg/s, $T_{in,water}$ = 298.15 K and M_{water} = 0.06 kg/s.

and ΔT of the absorber tube decrease with the increasing mass flow rate of the oil due to the increase in its convective heat transfer performance. Compared to the plain PTR, the T_{max} and ΔT of the PTR with double tube are apparently reduced and the reduction amplitudes of the T_{max} and ΔT decrease along with the increasing mass flow rate of the oil. It can be seen from Fig. 7 (c) that both the inlet temperature and mass flow rate of the water (LT-HTF) in the inner tube have little effect on the T_{max} and ΔT of the absorber tube. And the T_{max} and ΔT of the absorber tube perform a similar trend, as both of them decrease with the increasing mass flow rate of the water and the diminution of its inlet temperature.

4.2. Heat transfer and flow characteristics

Fig. 8 illustrates the effects of the inlet temperatures and mass flow rates of the oil and water on the heat transfer enhancement ratio (Nu/Nu_0) of the absorber tube inner surface and the flow resistance increase ratio (f/f_0) of the oil. In which, Nu_0 and f_0 are the Nusselt number and friction factor of the plain absorber tube. It is observed that the heat transfer coefficient on the absorber tube inner surface in a PTR with double tube is enhanced to about 1.5 times that of a plain PTR, and the flow resistance of the oil is increased to about 3.2–3.6 times that of the plain PTR. From Fig. 8 (a), as the oil inlet temperature increases, the Nu/Nu_0 goes down first and then up slightly, while the f/f_0 is brought down. Both the Nu/Nu_0 and f/f_0 decrease with the increasing mass flow rate of the oil, as shown in Fig. 8 (b). The Nu/Nu_0 and f/f_0 of the oil flow vary little with the water inlet temperature and mass flow rate in the inner tube, as shown in Fig. 8 (c). Among them, the Nu/Nu_0 decreases mildly with the increase of the inlet temperature and mass flow rate of the water. While the f/f_0 decreases slightly with the increasing inlet temperature and the decreasing mass flow rate of the water, because of the little increment of the oil temperature and reduction of its viscosity.

The pumping work is an important parameter of the PTR which represents the operating costs. Fig. 9 displays its variation with different parameters. The pumping work of the PTR with double tube (W_p) consists of two parts, including the pumping work of the oil between the absorber and inner tubes ($W_{p,\ oil}$) and the pumping work of the water in the inner tube ($W_{p,\ water}$). From Fig. 9 (a), it's observed that $W_{p,\ oil}$ performs a tendency to decrease first and then increase as the inlet temperature of the oil increases, while the variation of the $W_{p,\ water}$ with $T_{in,\ oil}$ is limited. Thus, the W_p shows the similar trend to the $W_{p,\ oil}$. Moreover, the pumping work of the PTR (W_{p0}) increases with the increasing $T_{in,\ oil}$, and the pumping work ratio (W_p/W_{p0}) decreases from 3.98 to 3.36. From Fig. 9 (b), it can be seen that as the mass flow rate of the oil increases, all the W_p, $W_{p,\ oil}$ and W_{p0} increase, while the $W_{p,\ water}$ remains basically unchanged. In addition, the W_p/W_{p0} decreases with the increase of the oil mass flow rate. It clear that the effects of the water inlet temperature and mass flow rate on the $W_{p,\ oil}$ are limited, as shown in Fig. 9 (c). And the enlarged graph in Fig. 9 (c) illustrates that the $W_{p,\ oil}$ shows the similar tendency to the f/f_0 in Fig. 8 (c). Both $W_{p,\ water}$ and W_p/W_{p0} increase with the increasing mass flow rate and decreasing inlet temperature of the water.

4.3. Heat collecting performance

Heat collecting efficiency and heat loss are the major performance of the PTR. Fig. 10 illustrates the variations of the heat collecting efficiency and heat loss with different parameters. The optical efficiency of the LS2 PTC applied in this study is set to 73.1%. In other words, 26.9% of the incident solar energy is lost in the form of optical loss. Thus, the sum of the collecting heat and heat loss accounts for 73.1% of the total incident solar energy. As a result, the heat collecting efficiency and the heat loss show opposite trend versus parameters, as it can be seen in Fig. 10. As the $T_{in,\ oil}$ increases and M_{oil} decreases, the heat loss increases due to the temperature increase of the absorber tube, and the heat collecting efficiency decreases consequently, as shown in Fig. 10 (a) and (b). The reduction in heat loss reaches up to 76.7 W/m and the maximum reduction rate of the heat loss is up to 43.1% when compared to the plain PTR. Moreover, compared to the plain PTR, the heat collecting efficiency of the PTR with double tube obtains an effective improvement up to 1.5%, and the enhancement of the efficiency decreases with the increasing M_{oil}. From Fig. 10(c), it is observed that the efficiency increases slightly with the decreasing $T_{in,\ water}$ and the increasing M_{water}. But the effects of the $T_{in,\ water}$ and M_{water} on the heat loss and heat collecting efficiency are limited.

Considering that the distribution of the collecting heat in oil (high temperature) and water (low temperature) is an important characteristic for the solar cascade heat collection system, Fig. 11 gives the proportion of the solar energy in different parts, such as high temperature heat gain, low temperature heat gain and heat loss, and their variations with different parameters. Though the total heat gain of the PTR with double tube is higher than that of the plain PTR, the high temperature heat gain of the PTR with double tube is lower than that of the plain PTR, as part of the heat gain in PTR with double tube is assigned to the water (LT-HTF). The low temperature heat gain accounts for 8.86–28.37% of the incident

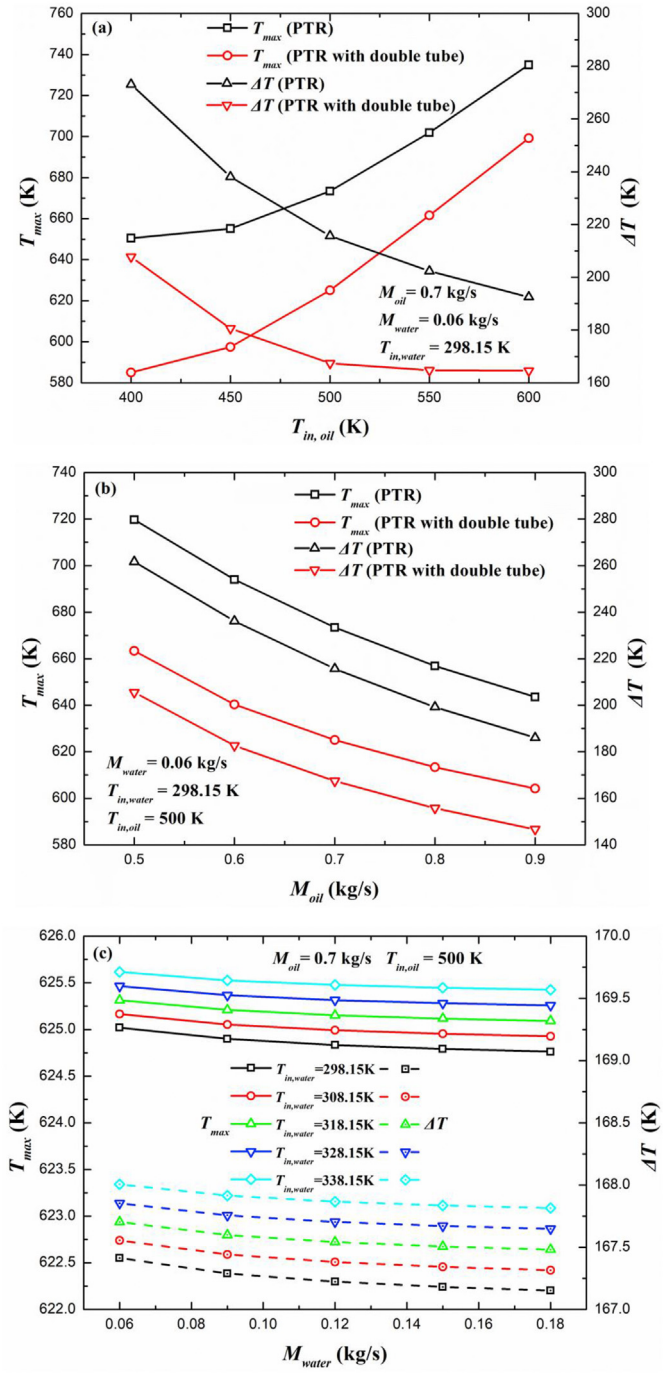

Fig. 7. Effects of different parameters on the maximum temperature (T_{max}) and temperature difference (ΔT) of the absorber tube: (a) inlet temperature of the oil; (b) mass flow rate of the oil; (c) inlet temperature and mass flow rate of the water.

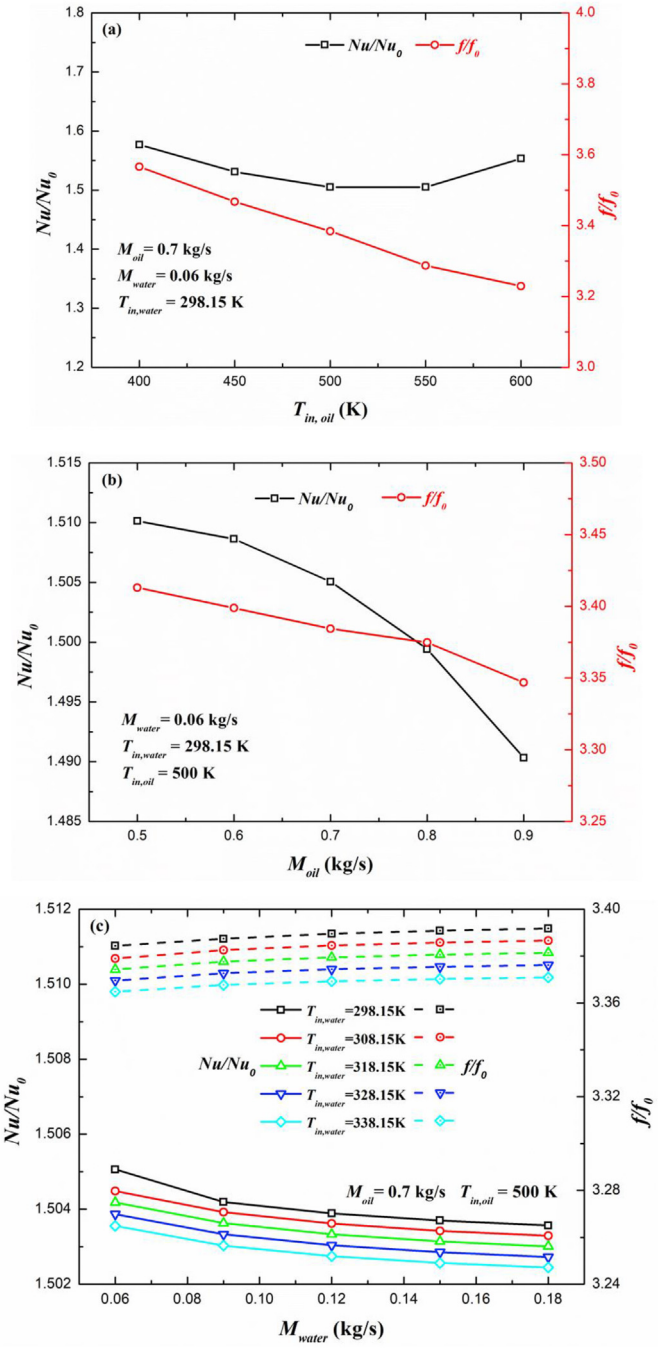

Fig. 8. Effects of different parameters on the heat transfer enhancement ratio (Nu/Nu_0) and the flow resistance increase ratio (f/f_0): (a) inlet temperature of the oil; (b) mass flow rate of the oil; (c) inlet temperature and mass flow rate of the water.

solar energy, while the high temperature heat gain accounts for 39.01–62.92% of the incident solar energy. Because the thermal-conduction resistance of the inner tube dominates the heat exchange resistance between the oil and water, the mass flow rates of the oil and water have little influence on the distribution of the collecting heat, as shown in Fig. 11 (b) and (c). While the inlet temperatures of the oil and water can affect the temperature difference between the oil and water. Thus, they have relatively greater effect on the distribution of the collecting heat than mass flow rates. It can be seen that the proportion of low temperature heat gain increases with the increasing $T_{in,\,oil}$ and the decreasing $T_{in,\,water}$ in Fig. 11 (a) and (c). At the same time, the proportion of high temperature heat gain decreases.

To characterize the quality of the collecting heat, Fig. 12 illustrates the temperature gains of the HTFs at different inlet temperatures and mass flow rates of the HTFs. It is indicated from Fig. 12 (a) that as the $T_{in,\,oil}$ increases, the oil temperature gains in the plain PTR and PTR with double tube decrease from 21.7 to 17.2 K and 19.3 to 10.1 K, respectively, while the water temperature gain in

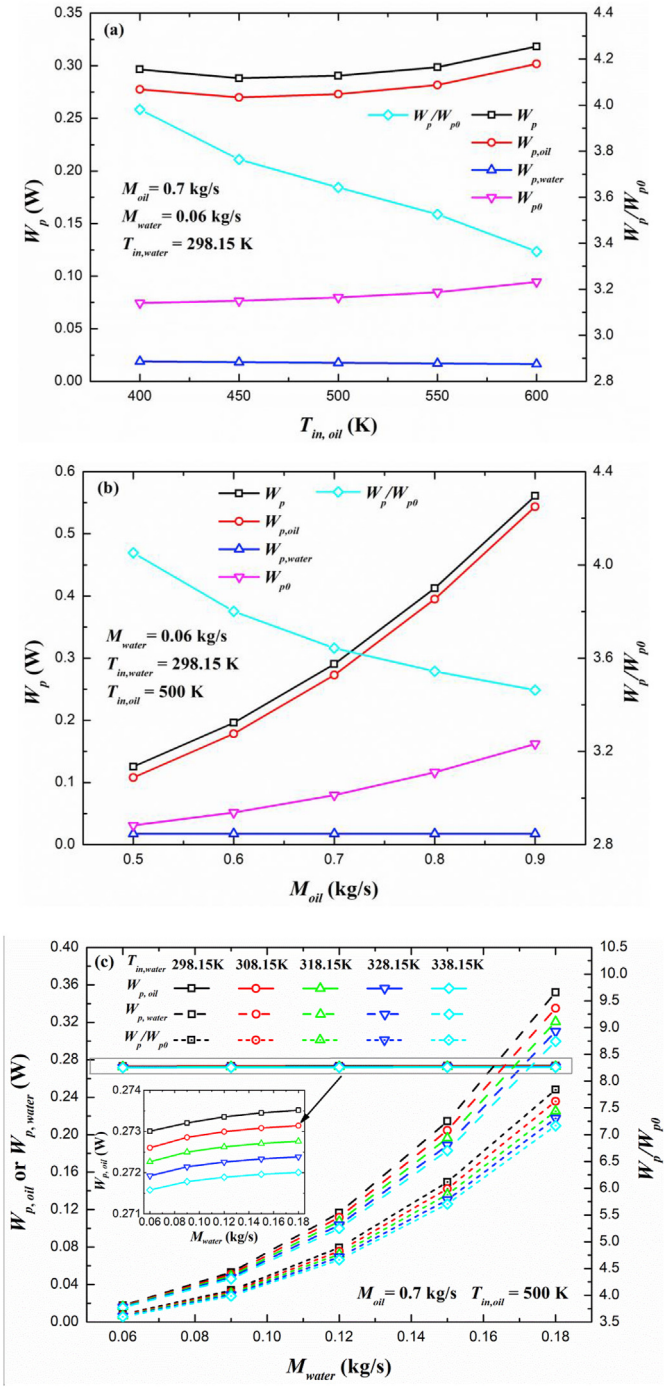

Fig. 9. The pumping work of the plain PTR and PTR with double tube versus different parameters: (a) inlet temperature of the oil; (b) mass flow rate of the oil; (c) inlet temperature and mass flow rate of the water.

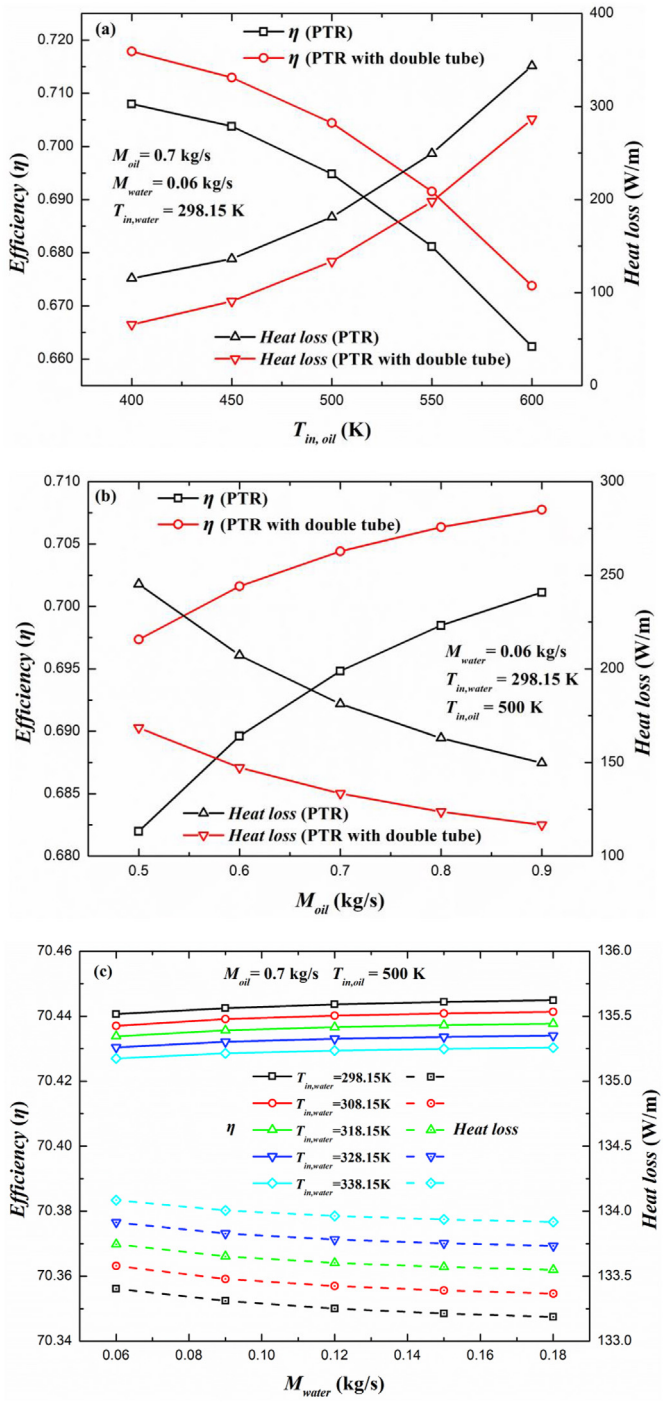

Fig. 10. The heat collecting efficiency and heat loss versus different parameters: (a) inlet temperature of the oil; (b) mass flow rate of the oil; (c) inlet temperature and mass flow rate of the water.

PTR with double tube increases relatively faster from 13.8 to 44.2 K. As the M_{oil} increases, both the oil temperature gains in the plain PTR and PTR with double tube decrease and the water temperature gain increases slightly, as shown in Fig. 12 (b). The inlet temperature and mass flow rate of the water have little effect on the oil temperature gain but great influence on the water temperature gain, as it can been seen in Fig. 12 (c). Both the oil and water temperature gains decrease with the increasing M_{water}. And as the $T_{in,\ water}$ increases, the oil temperature gain increases and the water temperature gain decreases. Overall, the temperature gains of the HTFs are mainly affected by their own mass flow rates and their temperature difference, while the mass flow rate of each HTF has little effect on the temperature gain of another HTF.

4.4. Comparison with literatures

Fig. 13(a)-(c) present the comparisons of the enhancements in

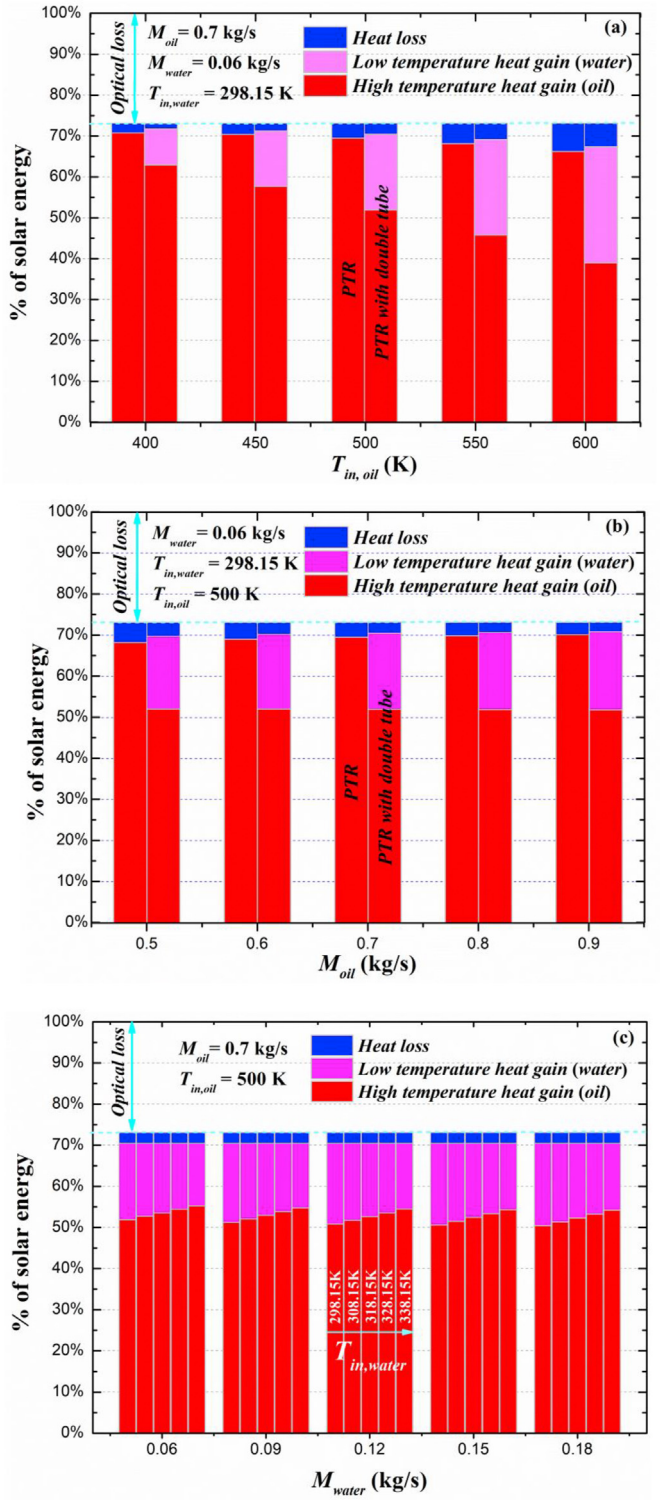

Fig. 11. Distribution of the solar energy in different parts and their variation versus different parameters: (a) inlet temperature of the oil; (b) mass flow rate of the oil; (c) inlet temperature and mass flow rate of the water.

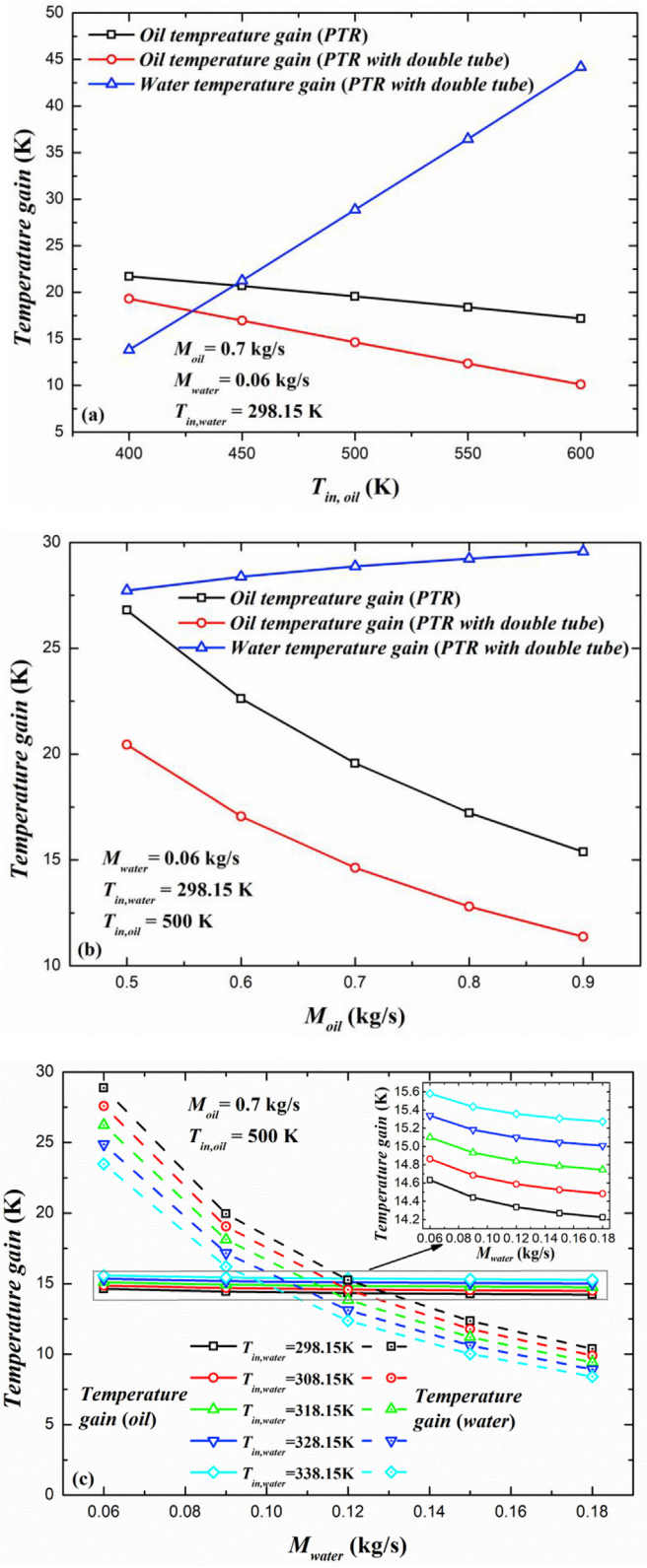

Fig. 12. Temperature gains of the HTFs versus different parameters: (a) inlet temperature of the oil; (b) mass flow rate of the oil; (c) inlet temperature and mass flow rate of the water.

heat transfer performance, pumping work and thermal efficiency with literatures [16,56] which applied the same heat transfer fluid (Syltherm-800 oil) and the similar range of fluid inlet temperatures. From Fig. 13 (a), it is observed that the increase in heat transfer performance of double tube in the present study is higher than smooth PTR with nanofluid but lower than different types of finned absorbers. It is indicated in Fig. 13 (b) that the increase in pumping

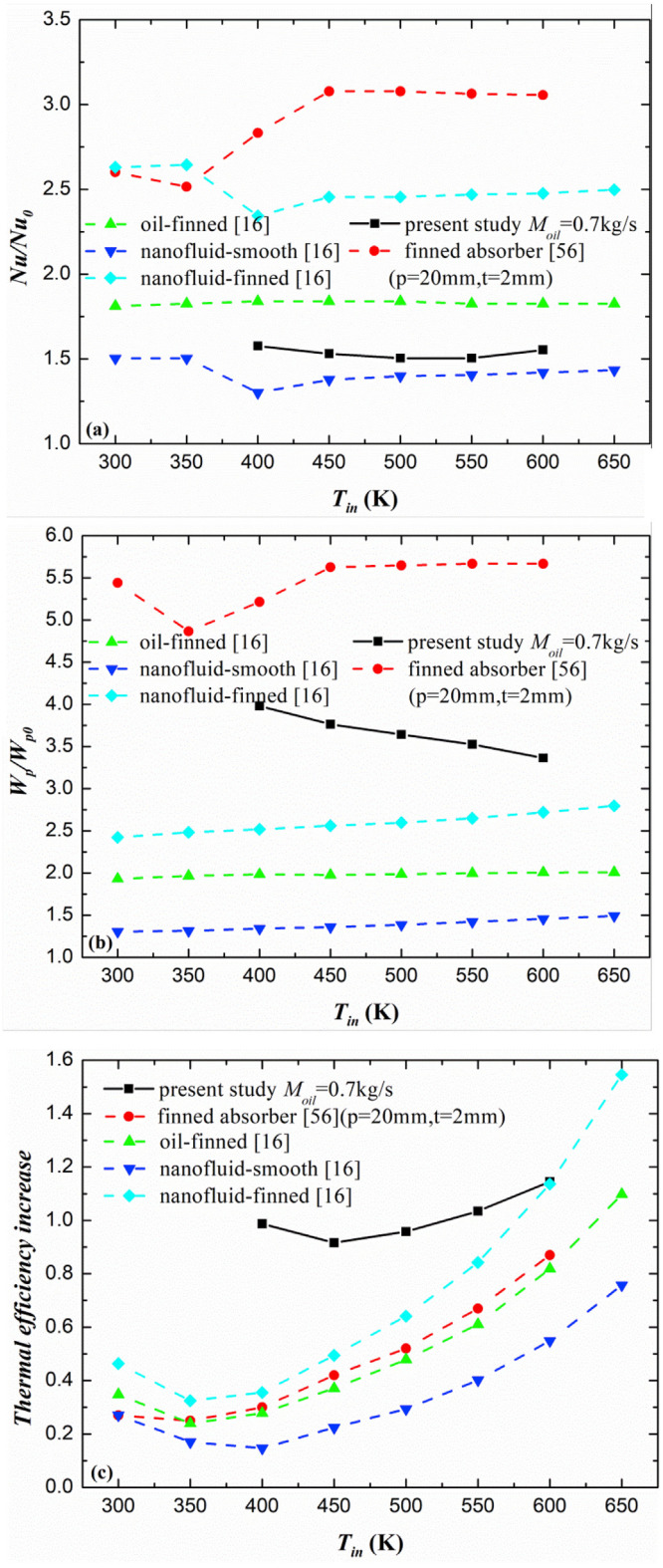

Fig. 13. Comparisons with literatures: (a) Nu/Nu_0; (b) W_p/W_{p0}; (c) increase in thermal efficiency.

work of this study is located in a moderate range. Moreover, the present work obtains the highest enhancement in thermal efficiency when compared with literatures, as shown in Fig. 13 (c).

5. Conclusions

A novel PTR with double tube based on LS2 PTC for solar cascade heat collection is proposed in this study. And a three-dimensional model has been developed to simulate and analyze the thermal-hydraulic and heat collecting performance of the PTR with double tube and two HTFs. In addition, the effects of the operating parameters (eg. inlet temperatures and mass flow rates of the oil and water) on the performance have been investigated in detail. Based on the study and analysis, the main conclusions can be drawn as follows:

(1) The insertion of the inner tube compresses the cross-sectional area of the HT-HTF (oil) and increases the velocity of the oil. As a result, the heat flux loaded on the absorber tube can be taken away more rapidly and the peak temperature and circumferential temperature gradient of the absorber tube are apparently reduced when compared to a plain PTR at the same oil mass flow rate. The maximum temperature and temperature difference of the absorber tube are reduced up to 66 K and 65 K, respectively. And they are greatly influenced by the inlet temperature and mass flow rate of the oil, but weakly affected by the inlet temperature and mass flow rate of the water in the inner tube.

(2) Compared to the plain PTR, the heat transfer coefficient on the absorber tube inner surface in a PTR with double tube is enhanced about 50%, while the flow resistance of the oil is increased 220–260%. Analysis on the pumping work has been carried out, and the results indicate that the pump power consumptions of the oil flow and water flow are mainly affected by their own mass flow rates. In addition, the total pumping work of the PTR with double tube is increased to 3.5–7.8 times that of the plain PTR at the same oil mass flow rate.

(3) The PTR with double tube obtains heat loss reduction up to 76.7 W/m and the maximum reduction rate of the heat loss reaches up to 43.1%, when compared to the plain PTR. The PTR with double tube obtains an effective improvement up to 1.5% in total heat collecting efficiency compared to the plain PTR. Moreover, the efficiency increases with the increasing M_{oil} and the decreasing $T_{in,\ oil}$, while it is less affected by the $T_{in,\ water}$ and M_{water} in the inner tube.

(4) The distribution of the collecting heat in HT-HTF and LT-HTF is less influenced by the mass flow rates of the oil and water, because the thermal-conduction resistance of the inner tube is the predominant resistance of the heat exchange between the oil and water. In addition, the proportion of low temperature heat gain increases as the temperature difference between the oil and water increases (increase of oil inlet temperature or decrease of water inlet temperature), which is ranged in 8.86–28.37% of the incident solar energy. In contrast, the proportion of high temperature heat gain decreases from 62.92% to 39.01% of the incident solar energy. The mass flow rates of the oil and water have significant effect on their own temperature gains, which represent the grade of the collecting heat. While the mass flow rate of each HTF has little effect on the temperature gain of another HTF. The temperature gains of the oil and water are ranged in 10.1–20.4 K and 8.4–44.2 K, respectively.

Credit author statement

Peng Liu, Conceptualization; Methodology; Validation; Formal analysis; Investigation; Data curation; Writing – original draft;

Writing – review & editing. Zhimin Dong, Methodology; Validation; Formal analysis; Investigation; Data curation; Writing – review & editing. Hui Xiao, Methodology; Formal analysis; Investigation; Data curation; Writing – review & editing. Zhichun Liu, Resources; Supervision; Project administration. Wei Liu: Conceptualization; Resources; Supervision; Project administration; Funding acquisition.

Declaration of competing interest

The authors declare that they have no known competing financial interests or personal relationships that could have appeared to influence the work reported in this paper.

Acknowledgment

The work was supported by the National Natural Science Foundation of China (Grant No. 51736004), the National Natural Science Foundation of China (51376069).

References

[1] Fuqiang W, Ziming C, Jianyu T, Yuan Y, Yong S, Linhua L. Progress in concentrated solar power technology with parabolic trough collector system: a comprehensive review. Renew Sustain Energy Rev 2017;79:1314–28.
[2] Akbarzadeh S, Valipour MS. Heat transfer enhancement in parabolic trough collectors: a comprehensive review. Renew Sustain Energy Rev 2018;92:198–218.
[3] Bellos E, Tzivanidis C. Alternative designs of parabolic trough solar collectors. Prog Energy Combust Sci 2019;71:81–117.
[4] Yılmaz İH, Mwesigye A. Modeling, simulation and performance analysis of parabolic trough solar collectors: a comprehensive review. Appl Energy 2018;225:135–74.
[5] Kumaresan G, Sudhakar P, Santosh R, Velraj R. Experimental and numerical studies of thermal performance enhancement in the receiver part of solar parabolic trough collectors. Renew Sustain Energy Rev 2017;77:1363–74.
[6] Armaroli N, Balzani V. Energy for a Sustainable world. Weinheim: Wiley-VCH; 2011.
[7] Barlev D, Vidu R, Stroeve P. Innovation in concentrated solar power. Sol Energy Mater Sol Cell 2011;95(10):2703–25.
[8] Hafez AZ, Attia AM, Eltwab HS, ElKousy AO, Afifi AA, AbdElhamid AG, AbdElqader AN, Fateen SEK, El-Metwally KA, Soliman A, Ismail IM. Design analysis of solar parabolic trough thermal collectors. Renew Sustain Energy Rev 2018;82:1215–60.
[9] Sandeep HM, Arunachala UC. Solar parabolic trough collectors: a review on heat transfer augmentation techniques. Renew Sustain Energy Rev 2017;69:1218–31.
[10] Mwesigye A, Bello-Ochende T, Meyer JP. Numerical investigation of entropy generation in a parabolic trough receiver at different concentration ratios. Energy 2013;53:114–27.
[11] Mwesigye A, Bello-Ochende T, Meyer JP. Minimum entropy generation due to heat transfer and fluid friction in a parabolic trough receiver with non-uniform heat flux at different rim angles and concentration ratios. Energy 2014;73:606–17.
[12] Lei D, Li Q, Wang Z, Li J, Li J. An experimental study of thermal characterization of parabolic trough receivers. Energy Convers Manag 2013;69:107–15.
[13] Lei D, Fu X, Ren Y, Yao F, Wang Z. Temperature and thermal stress analysis of parabolic trough receivers. Renew Energy 2019;136:403–13.
[14] Wu Z, Lei D, Yuan G, Shao J, Zhang Y, Wang Z. Structural reliability analysis of parabolic trough receivers. Appl Energy 2014;123:232–41.
[15] Manikandan GK, Iniyan S, Goic R. Enhancing the optical and thermal efficiency of a parabolic trough collector – a review. Appl Energy 2019;235:1524–40.
[16] Bellos E, Tzivanidis C, Tsimpoukis D. Enhancing the performance of parabolic trough collectors using nanofluids and turbulators. Renew Sustain Energy Rev 2018;91:358–75.
[17] Mwesigye A, Huan Z, Meyer JP. Thermodynamic optimisation of the performance of a parabolic trough receiver using synthetic oil–Al2O3 nanofluid. Appl Energy 2015;156:398–412.
[18] Malekan M, Khosravi A, Syri S. Heat transfer modeling of a parabolic trough solar collector with working fluid of Fe3O4 and CuO/Therminol 66 nanofluids under magnetic field. Appl Therm Eng 2019;163:114435.
[19] Mwesigye A, Huan Z, Meyer JP. Thermal performance and entropy generation analysis of a high concentration ratio parabolic trough solar collector with Cu-Therminol®VP-1 nanofluid. Energy Convers Manag 2016;120:449–65.
[20] Bellos E, Tzivanidis C, Tsimpoukis D. Thermal, hydraulic and exergetic evaluation of a parabolic trough collector operating with thermal oil and molten salt based nanofluids. Energy Convers Manag 2018;156:388–402.
[21] Mohammad Zadeh P, Sokhansefat T, Kasaeian AB, Kowsary F, Akbarzadeh A. Hybrid optimization algorithm for thermal analysis in a solar parabolic trough collector based on nanofluid. Energy 2015;82:857–64.
[22] Kasaeian A, Daviran S, Azarian RD, Rashidi A. Performance evaluation and nanofluid using capability study of a solar parabolic trough collector. Energy Convers Manag 2015;89:368–75.
[23] Verma SK, Tiwari AK. Progress of nanofluid application in solar collectors: a review. Energy Convers Manag 2015;100:324–46.
[24] Jaramillo OA, Borunda M, Velazquez-Lucho KM, Robles M. Parabolic trough solar collector for low enthalpy processes: an analysis of the efficiency enhancement by using twisted tape inserts. Renew Energy 2016;93:125–41.
[25] Mwesigye A, Bello-Ochende T, Meyer JP. Multi-objective and thermodynamic optimisation of a parabolic trough receiver with perforated plate inserts. Appl Therm Eng 2015;77:42–56.
[26] Zhu X, Zhu L, Zhao J. Wavy-tape insert designed for managing highly concentrated solar energy on absorber tube of parabolic trough receiver. Energy 2017;141:1146–55.
[27] Liu P, Zheng N, Liu Z, Liu W. Thermal-hydraulic performance and entropy generation analysis of a parabolic trough receiver with conical strip inserts. Energy Convers Manag 2019;179:30–45.
[28] Song X, Dong G, Gao F, Diao X, Zheng L, Zhou F. A numerical study of parabolic trough receiver with nonuniform heat flux and helical screw-tape inserts. Energy 2014;77:771–82.
[29] Bellos E, Tzivanidis C, Daniil I, Antonopoulos KA. The impact of internal longitudinal fins in parabolic trough collectors operating with gases. Energy Convers Manag 2017;135:35–54.
[30] Cheng ZD, He YL, Cui FQ. Numerical study of heat transfer enhancement by unilateral longitudinal vortex generators inside parabolic trough solar receivers. Int J Heat Mass Tran 2012;55(21):5631–41.
[31] Fuqiang W, Qingzhi L, Huaizhi H, Jianyu T. Parabolic trough receiver with corrugated tube for improving heat transfer and thermal deformation characteristics. Appl Energy 2016;164:411–24.
[32] Fuqiang W, Zhexiang T, Xiangtao G, Jianyu T, Huaizhi H, Bingxi L. Heat transfer performance enhancement and thermal strain restrain of tube receiver for parabolic trough solar collector by using asymmetric outward convex corrugated tube. Energy 2016;114:275–92.
[33] Liu P, Lv J, Shan F, Liu Z, Liu W. Effects of rib arrangements on the performance of a parabolic trough receiver with ribbed absorber tube. Appl Therm Eng 2019;156:1–13.
[34] Muñoz J, Abánades A. Analysis of internal helically finned tubes for parabolic trough design by CFD tools. Appl Energy 2011;88(11):4139–49.
[35] Chang C, Sciacovelli A, Wu Z, Li X, Li Y, Zhao M, Deng J, Wang Z, Ding Y. Enhanced heat transfer in a parabolic trough solar receiver by inserting rods and using molten salt as heat transfer fluid. Appl Energy 2018;220:337–50.
[36] Bellos E, Tzivanidis C, Tsimpoukis D. Multi-criteria evaluation of parabolic trough collector with internally finned absorbers. Appl Energy 2017;205:540–61.
[37] Abdulhamed AJ, Adam NM, Ab-Kadir MZA, Hairuddin AA. Review of solar parabolic-trough collector geometrical and thermal analyses, performance, and applications. Renew Sustain Energy Rev 2018;91:822–31.
[38] Sharon H, Reddy KS. A review of solar energy driven desalination technologies. Renew Sustain Energy Rev 2015;41:1080–118.
[39] Andrés-Mañas JA, Roca L, Ruiz-Aguirre A, Acién FG, Gil JD, Zaragoza G. Application of solar energy to seawater desalination in a pilot system based on vacuum multi-effect membrane distillation. Appl Energy 2020;258:114068.
[40] Zheng Y, Hatzell KB. Technoeconomic analysis of solar thermal desalination. Desalination 2020;474:114168.
[41] Omar A, Nashed A, Li Q, Leslie G, Taylor RA. Pathways for integrated concentrated solar power - desalination: A critical review. Renew Sustain Energy Rev 2020;119:109609.
[42] Gunawan A, Simmons RA, Haynes MW, Moreno D, Menon AK, Hatzell MC, Yee SK. Techno-economics of cogeneration approaches for combined power and desalination from concentrated solar power. J Sol Energy Eng 2019;141(2).
[43] Long R, Kuang Z, Liu Z, Liu W. Ionic thermal up-diffusion in nanofluidic salinity-gradient energy harvesting. National Science Review 2019;6(6):1266–73.
[44] He Y-L, Xiao J, Cheng Z-D, Tao Y-B. A MCRT and FVM coupled simulation method for energy conversion process in parabolic trough solar collector. Renew Energy 2011;36(3):976–85.
[45] Bejan A. Convection heat transfer. John Wiley & Sons; 2013.
[46] Qiu Y, Zhang Y, Li Q, Xu Y, Wen Z-X. A novel parabolic trough receiver enhanced by integrating a transparent aerogel and wing-like mirrors. Appl Energy 2020;279:115810.
[47] Nait-Ali B, Haberko K, Vesteghem H, Absi J, Smith DS. Preparation and thermal conductivity characterisation of highly porous ceramics: comparison between experimental results, analytical calculations and numerical simulations. J Eur Ceram Soc 2007;27(2):1345–50.
[48] Mullick SC, Nanda SK. An improved technique for computing the heat loss factor of a tubular absorber. Sol Energy 1989;42(1):1–7.
[49] Forristall R. Heat transfer analysis and modeling of a parabolic trough solar receiver implemented in engineering equation solver. 2003. NREL/TP-550-34169.
[50] Mwesigye A, Bello-Ochende T, Meyer JP. Heat transfer and thermodynamic performance of a parabolic trough receiver with centrally placed perforated plate inserts. Appl Energy 2014;136:989–1003.

[51] Fluent incorporated, user's guide for FLUENT/UNS and RAMPANT. Fluent Incorporated, Lebanon, NH 03766, USA Release 4.0 1996;1(2, and 4).
[52] Shih T-H, Liou WW, Shabbir A, Yang Z, Zhu J. A new k-ε eddy viscosity model for high Reynolds number turbulent flows. Comput Fluid 1995;24(3):227–38.
[53] Liu P, Dong Z, Lv J, Shan F, Liu Z, Liu W. Numerical study on thermal-hydraulic performance and exergy analysis of laminar oil flow in a circular tube with fluid exchanger inserts. Int J Therm Sci 2020;153:106365.
[54] Incropera PDWFP, Bergman TL, Lavine AS. Fundamentals of heat and mass transfer. sixth ed. John-Wiley & Sons; 2006.
[55] Dudley EV SM, Kolb JG, Kearney D. SEGS LS2 solar collector-test results. Report of Sandia National Laboratories; 1994.
[56] Bellos E, Tzivanidis C, Tsimpoukis D. Thermal enhancement of parabolic trough collector with internally finned absorbers. Sol Energy 2017;157:514–31.